Model-Free Predictive Control Based on Data-Driven for Fast and Accurate Power Allocation in Solid-State DC Transformers

Dehao Kong, *Graduate Student Member, IEEE*, Shaobin Li, Chuang Liu, *Member, IEEE*, Zhenbin Zhang, *Senior Member, IEEE*, Yuanxiang Sun, *Graduate Student Member, IEEE*, Ralph Kennel, *Life Senior Member, IEEE*, and Marcelo Lobo Heldwein, *Senior Member, IEEE*

***Abstract*—Robustness is a crucial issue in model predictive control despite the excellent dynamic performance and effective management of multiple variables that this control strategy provides for converters. This challenge is particularly concerning in solid-state dc transformers (DCT) connected as input-series-output-parallel modules because this type of DCT not only regulates the output voltage/power but also balances the input voltage so that the power is averagely distributed among submodules. Static errors and limited dynamics pose a threat to their operation and even safety. To tackle this issue, this article proposes a novel model-free predictive control based on an autoregressive moving average structure. Herein, the physical model of DCTs is completely replaced by a data-driven model. Combined with the recursive least square method with the forgetting factor, the control system will no longer rely on the electrical parameters, guaranteeing strong robustness. Meanwhile, an adaptive balance controller is also proposed, which adjusts the gain of shift angles with reduced computational burden. These achieve accurate power/voltage allocation among all submodules while maintaining a fast dynamic response. The experimental comparisons with other schemes verify the effectiveness and superiority of the proposed method.**

***Index Terms*—Adaptive balance controller, model-free predictive control (MFPC), solid-state dc transformer (DCT).**

Nomenclature

β_1, β_2	Error feedback gains of ESO.
Δ	System's lumped disturbance.
η	Slope of adjusting term.
γ_0	Mid-point of Sigmoid function.
λ	Forgetting factor.
ω_n	Bandwidth of ESO.
θ, ϕ	ARMA coefficients.
C_{oi}	Capacitor of output port of ith DAB.
f_s	Switching frequency.
I_{2i}	Output current of ith DAB.
I_{2n}	Normalized output current.
I_{2r}	Base value of output current.
I_{oi}	Load current of ith DAB.
L_k	Leakage inductor of HFT.
N	Number of modules.
p	Orders of autoregressive part.
q	Orders of moving average part.
u	Control signal.
u_{filt}	Filterd control signal.
U_{in}	Input voltage.
U_o	LVDC voltage.
u_{bali}	Final control signal for ith DAB.
U_{ini}	Input voltage of ith DAB.
z_1	Observed output voltage.
z_2	Disturbance.

Received 27 February 2024; revised 5 July 2024; accepted 16 August 2024. Date of publication 22 August 2024; date of current version 12 December 2024. Recommended for publication by Associate Editor H. S.-H. Chung. *(Corresponding author: Shaobin Li.)*

Dehao Kong, Yuanxiang Sun, Ralph Kennel, and Marcelo Lobo Heldwein are with the Chair of High-Power Converter Systems, Technical University of Munich, 80333 Munich, Germany (e-mail: dehao.kong@tum.de; yuanxiang.sun@tum.de; ralph.kennel@tum.de; marcelo.heldwein@tum.de).

Shaobin Li is with the School of Electrical Engineering and Automation, Harbin Institute of Technology, Harbin 150001, China (e-mail: flyingshaobin@stu.hit.edu.cn).

Chuang Liu is with the School of Electrical Engineering, Northeast Electric Power University, Jilin 132012, China (e-mail: 20122440@neepu.edu.cn).

Zhenbin Zhang is with the School of Electrical Engineering, Shandong University, Jinan 250061, China (e-mail: zbz@sdu.edu.cn).

Color versions of one or more figures in this article are available at https://doi.org/10.1109/TPEL.2024.3448243.

Digital Object Identifier 10.1109/TPEL.2024.3448243

I. Introduction

With the fast development of medium-voltage dc (MVDC) systems, MV solid-state dc transformers (DCT), serving as key-equipment at power distribution notes, have gained numerous interests [1], [2], [3]. Such a power electronics-based equipment not only offers the fundamental functions of galvanic isolation and dc conversion but also provides additional smart functions, such as active voltage/power transformation/support and the ability of optimal power management [3], [4], [5]. These advantages benefit nodes in the distribution system and improve their autonomies.

In this MV-rated application, DCTs are to be constructed through a modular structure due to power semiconductors' voltage limitations and maximum current ratings. Among the alternative topologies, the dual active bridge (DAB) converters connected in an input-series-output-parallel (ISOP) structure are one of the most promising schemes due to their 1) expandability, 2) high controllability, and 3) no requirement of line/medium

frequency transformers, among other attractive features [6], [7], [8].

To pursue benefits, such as outstanding dynamic performance and the ability to accommodate multiple objectives, model predictive control (MPC), recognized as an advanced controller, has been applied to DCTs in recent years [8], [9], [10], [11], [12]. Its fast dynamic response, proficiency in managing multiple variables, and the adaptability to customer-designed cost functions position MPC as a promising control method for DCTs. Chen et al.[13] proposed a single-phase shift modulation-based MPC for a single DAB converter, enhancing its dynamic performance. In [10], a similar method was applied to a DCT, simultaneously controlling the output and balancing the input power. The authors in [8] and [11] combined multiphase shift modulation with MPC, pursuing further optimizations for the efficiency and current stress.

However, MPC performance highly relies on the accurate modeling and parameters, which is a crucial issue that probably slows its applications in DCTs. Theoretically, MPC predicts the states of switches in the next step based on the sampling value and the known discrete model, thereby achieving the fast dynamic and optimization of multiple targets [9]. Nevertheless, inaccuracy models, neglected dead times, and parameter errors degrade controller's performance, which leads to static errors of reference tracking and incompetent dynamic performance [14]. This concern becomes particularly pronounced in the context of ISOP-type DCTs. These DCTs require balance controllers for the input voltage among all submodules, preventing power allocation bias caused by the small differences (mainly about inductors) between each module [15], [16]. Such biases will increase the electrical and thermal stresses on partial DABs, decreasing the system reliability and even damaging the system if the bias continuously accumulates. Any static error and incompetent dynamic response will hinder this balance control and potentially threaten the safety of DCTs.

Some previous works attempted to address this issue with model-based solutions, for example, disturbance observer-based (DOB) methods and online parameter identification schemes. DOB methods exploit a specially designed observer to estimate the deviations between the nominal model and the real plant, and the results are then used for compensation. In this group, Zhang et al. [8] adopted an extended state observer (ESO) for overall uncertainty estimation, whereas Wu et al. [17] addressed an uncertainty and disturbance estimator for robust voltage tracking control. On the contrary, parameter identification-based methods update the nominal model with accurately calculated parameters, canceling the influence caused by parameter mismatches. In [14] and [18], online identification of the leakage inductance is performed with the recursive least square (RLS) method and the control accuracy is improved.

However, the antidisturbance performance in the aforementioned methods is still affected by the use of a parametric model and it is hard for the model-based compensation techniques to completely eliminate the disturbance [14], [19], [20], [21]. To avoid the use of physical models, the model-free predictive control (MFPC) approach (also called data-driven) has been recently proposed in the field of power electronics. Various techniques have drawn tremendous attention, including ultra-local model-based MFPC methods with ESO [22], look-up table-based MFPC methods [23], neural-network-based adaptive predictive control methods [24], etc. Up till now, the applications of MFPC in DCTs have hardly been studied and the potential has not been fully exploited. Motivated by this thought, this article proposes a novel MFPC method based on an autoregressive moving average (ARMA) structure, completely eliminating the dependence on the physical model of DCTs while maintaining fast dynamic performance. Unlike tedious trial and error methods for order selection used in the previous works, the order of the ARMA structure is designed by an order selection method proposed in this work. Moreover, all the related coefficients can be online-updated using an RLS method with the forgetting factor (FFRLS). Therefore, the accuracy of the data-driven model can be maintained.

On the other hand, the balance control algorithms based on the full MPC, in previous works, mainly introduced the input voltage into the cost function [8], [10]. This regulates the output and achieves input balancing effectively, taking full inherent advantages of multiobjective optimization with MPC. However, solving this complex cost function results in a heavy computational burden, especially as the number of functions increases with the number of connected modules. Meanwhile, the robustness problem of the system is not addressed, as this method is still dependent on the system model and parameters. Once there are errors in the parameters, the input voltage will not be able to be balanced.

Therefore, a novel adaptive balance controller is also proposed in this article, which dynamically adapts the gain of the converter's shift angles using a nonlinear negative feedback strategy. Compared with the full MPC methods, this approach reduces the computational burden, making it suitable for methods like MFPC, which inherently involve high computational demands. Consequently, aiming for both of the input and output side, it combined with the proposed MFPC method, achieving fast dynamics and accurate power allocations (MFPC-APA).

The main contributions of this work are as follows.

1) A novel MFPC method for DCTs based on the ARMA model is proposed, along with the employment of FFRLS identification. An ESO-based data preprocessing design is accordingly introduced to acquire clean data and compensate one-step time delay. Meanwhile, a model order selection method based on the DCT predictive control system and time series analysis is put forward to guarantee model fitting accuracy. The dependence on physical parameters is eliminated while the rapid dynamics inherent to predictive control is upheld.
2) The mechanism of voltage balance failure in the submodules has been analyzed. A novel adaptive balance controller is proposed. Compared with the full MPC methods, this balance controller effectively balances the input voltage, while achieving higher robustness and less computational burden.

The rest of this article is organized as follows. In Section II, the system model and optimal modulation are described. Section III introduces the architecture and principle of the

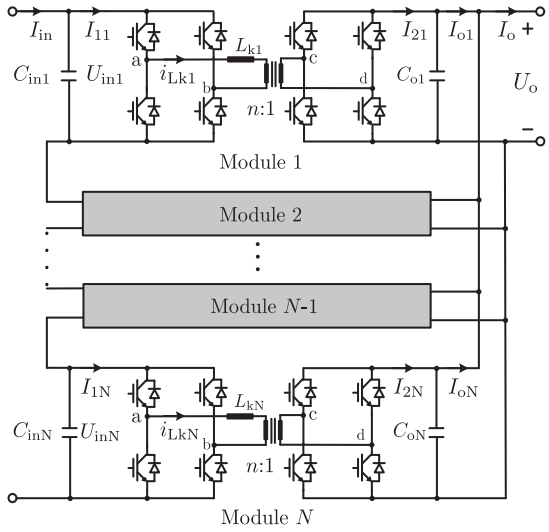

Fig. 1. Simplified topology of DCTs consisting of N DABs.

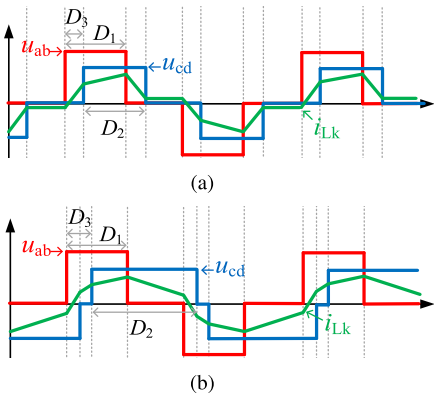

Fig. 2. Classic operation modes of DABs modulated by TPS. (a) Mode I. (b) Mode II.

proposed MFPC method. The balance controller and the implementation of the MFPC-APA are detailed in Section IV. The comparative experimental results are provided in Section V. Finally, Section VI concludes this article.

II. System Description, Modeling, and Modulation

Fig. 1 shows the simplified topology of DCTs consisting of N DABs, where each DAB consists of two H-bridges and one high-frequency transformer (HFT). The dynamic equation of output low-voltage dc (LVDC) port can be derived as follows:

$$\sum_{i=1}^{N} C_{oi}\frac{\mathrm{d}U_o}{\mathrm{d}t} = \sum_{i=1}^{N} I_{2i} - \sum_{i=1}^{N} I_{oi}. \tag{1}$$

Among the standard modulation strategies, the triple-phase shift (TPS) modulation possesses the highest degree of freedoms [25], [26]. There are many operation modes, i.e., the combination of shift angles, of DABs modulated by TPS. To purse the lowest current stress achieving high safety and high efficiency, normally only two modes are employed as shown in Fig. 2. As can be seen, u_{ab} and u_{cd} are the voltage of the primary side and the secondary side of HFT, respectively. i_{Lk} is the current of HFT. D_1, D_2, and D_3 are the shift angle of the primary side of HFT, the shift angle of the secondary side of HFT, and the shift angle between the two sides, respectively.

The output model of one single DAB for each operation mode, along with their optimal shift angles resulting in the lowest current stress, are listed in Table I. To simplify the analysis process, the output current is normalized by

$$I_{2n} = \frac{I_2}{I_{2r}}, I_{2r} = \frac{nU_{in}}{2f_sL_k} \tag{2}$$

where $m = \frac{nU_o}{U_{in}}$ is the voltage gain and n is the HFT turns-ratio, which is assumed as 1 to simplify the analysis.

It can be concluded from (1) and (2) that the models used by MPC are highly dependent on the parameters. Any inaccuracy will result in control errors, which can be even damaging the equipment, not to mention the errors of models themselves and the effects of dead time.

III. Model-Free Predictive Control Strategy for a Single DAB Converter

Instead of involving the overall DCT with N submodules, this section introduces the algorithm design for a single DAB to propose a clearer concept and consider the limited space. The entire system can be designed based on this method. The following part illustrates the data-driven model structure analysis, observer design, online coefficients identification, and control signals generation in detail.

A. ARMA Model Structure Analysis and Design

Until now, the model order selection method for the ARMA model in power electronics control has hardly been discussed. Existing literature usually choose the model order based on time-consuming trial and error with hardly any theoretical explanations. As a result, the fitting accuracy can be described as a matter of luck and cannot be guaranteed. In this part, a novel model order selection method based on the predictive control system and time series analysis is introduced.

The data-driven model of the DCT is designed in the ARMA structure, where the tracking error of the output voltage reference and the real value can be represented by the combination of the previous tracking error and the control input. Furthermore, a general ARMA(p, q) model can be written as follows:

$$\begin{aligned}\varepsilon(k+1) = {} & \phi_1\varepsilon(k) + \cdots + \phi_p\varepsilon(k-p+1) \\ & + \theta_0 + \theta_1\bar{u}(k+1) + \cdots + \theta_q\bar{u}(k+2-q)\end{aligned} \tag{3}$$

where p and q are positive integers representing the orders of autoregressive (AR) and moving average (MA) parts, respectively, $\varepsilon(k+1) = \hat{U}_o(k+1) - U_o^*(k+1)$ is the output voltage tracking error at time $t = k+1$, θ_x and ϕ_y $(x \in [0, 1, \ldots, q], y \in [1, \ldots, p])$ are ARMA coefficients to be determined, and $\bar{u}(k+1) = u(k)$ is the control signal calculated at $t = k-1$ while implemented at $t = k$.

It can be concluded that if the structure and coefficients are properly selected, the ARMA model above can approximate the

TABLE I
OUTPUT CURRENT AND OPTIMAL SHIFT ANGLES OF TPS

Mode	Current range	Output current	Optimal shift angles
I	$I_{2n} \in [0, \frac{m(1-m)}{2}]$	$I_{2\mathrm{n}} = \frac{1}{2}(D_1D_2 + 2D_1D_3 - D_1^2 - D_3^2)$	$D_1 = \sqrt{\frac{2mI_{2\mathrm{n}}}{(1-m)}}$, $D_2 = \frac{D_1}{m}$, $D_3 = 0$
II	$I_{2n} \in (\frac{m(1-m)}{2}, \frac{1}{4}]$	$I_{2\mathrm{n}} = \frac{1}{2}(D_1D_2 + 2D_1D_3 - 2D_2D_3 - D_1^2 - D_2^2 - 2D_3^2 + 2D_2 + 2D_3 - 1)$	$D_1 = 1 - (1-m)\sqrt{\frac{1-4I_{2\mathrm{n}}}{1-2m+2m^2}}$, $D_2 = 1$, $D_3 = \frac{D_1 - m}{2(1-m)}$

system model behavior with satisfying accuracy [19]. Accordingly, the predictive control law can be generated based on this data-driven model, which gets rid of all the electrical parameters so that strong robustness can be guaranteed.

As for the model structure, the ARMA model order can be selected by proper system and time series analysis. First, the MA order q represents the number of previous control signals $\bar{u}(k-q)$ that contribute to the formation of the present tracking error $\varepsilon(k)$. In this article, the deadbeat (DB) pattern is used. According to the generic DB design procedure considering time delay compensation [9], the kth output voltage $U_{\mathrm{o}}(k)$ is solely determined by $\bar{u}(k-1)$ and $\bar{u}(k-2)$, which has the expression as follows:

$$U_{\mathrm{o}}(k+2) = U_{\mathrm{o}}(k) + \frac{nU_{\mathrm{in}}}{2f_{\mathrm{s}}^2 L_{\mathrm{k}} C_{\mathrm{o}}}(\underbrace{I_{2\mathrm{n}}(k)}_{\bar{u}(k)} + \underbrace{I_{2\mathrm{n}}(k+1)}_{\bar{u}(k+1)}) - \frac{I_{\mathrm{o}}(k)}{f_{\mathrm{s}}C_{\mathrm{o}}} + \frac{\Delta(k)}{f_{\mathrm{s}}} - \frac{I_{\mathrm{o}}(k+1)}{f_{\mathrm{s}}C_{\mathrm{o}}} + \frac{\Delta(k+1)}{f_{\mathrm{s}}} \quad (4)$$

where $\Delta(k)$ denotes the system's lumped disturbance at time $t = k$. Hence, discarding all other controls before $\bar{u}(k-2)$ is reasonable when constructing the MA part and the resultant MA order can be chosen as 2 with good precision guaranteed.

The selection of the AR order p involves modeling the current value of the series as a linear combination of previous values (lags). The partial autocorrelation function (PACF) concept from time series analysis theory can be introduced to manifest the inherent characteristics of the system. The PACF value can be interpreted as the correlation between $\varepsilon(k)$ and $\varepsilon(k-p)$ without taking $\varepsilon(k-1)$, $\varepsilon(k-2)$,..., $\varepsilon(k-p+1)$ into account [27], [28], which can then be used to determine the AR model order. A set of system output tracking error data is acquired via simulation, serving as the time series data to be analyzed. Then, its PACF values corresponding to various lags, for example, from 1 to 20 in our demonstration, are calculated with respect to $\varepsilon(k)$. The calculation is performed using Python ("statsmodels" library) [27] and the PACF results of the time series data are presented in Fig. 3 for inspection. The height of each bar is in proportion to the relationship between $\varepsilon(k)$ and $\varepsilon(k-l)$ (l means lag number). Furthermore, a significance threshold is chosen, which means that lags with PACF values within this threshold are regarded as insignificant and can be cutoff. Therefore, only lags with PACF values exceeding this significant threshold will be considered in our design, and satisfactory accuracy can still be achieved. It is apparent that $p = 5$ is an appropriate choice considering model accuracy and calculation burden in our design, which can be testified by both simulation and experiments.

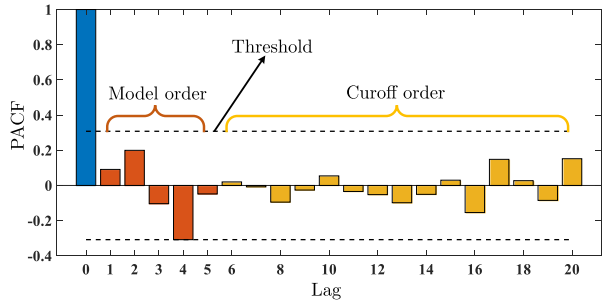

Fig. 3. PACF graph of voltage tracking error $\varepsilon(k)$.

B. Observer Design

The quality of data is crucial for data-driven methods, as a well-designed data acquisition method improves both the model and the control accuracy. To mitigate the unexpected noise in the sampling process, an ESO is incorporated into the proposed method. Moreover, this observer can reduce the data-driven model's order in the one-step delay compensation design [21]. By this technique, an accurate prediction of state variables for the next sampling period $t = k+1$ can be estimated, which is then used for the coefficients identification of the data-driven model. The expression of ESO is

$$\begin{cases} \dot{z}_1 = bu + z_2 + \beta_1(U_{\mathrm{o}} - z_1) \\ \dot{z}_2 = \beta_2(U_{\mathrm{o}} - z_1) \end{cases} \quad (5)$$

where $z_1 = U_{\mathrm{o}}$, z_2 is the estimated system's lumped disturbances and the input gain $b = \frac{nU_{\mathrm{in}}}{2f_{\mathrm{s}}L_{\mathrm{k}}C_{\mathrm{o}}}$.

The error feedback gains β_1 and β_2 can be designed according to the desired bandwidth ω_n as (6). Note that ω_n strongly relates to the observation performance. With a lower ω_n, a more obvious filtering effect

$$\begin{cases} \beta_1 = 2\omega_n \\ \beta_2 = {\omega_n}^2. \end{cases} \quad (6)$$

After discretization, (5) can be written as follows:

$$\begin{cases} z_1(k+1) = z_1(k) + T_{\mathrm{s}} \cdot bu(k) + T_{\mathrm{s}} \cdot z_2(k) \\ \qquad\qquad + T_{\mathrm{s}} \cdot \beta_1(U_{\mathrm{o}}(k) - z_1(k)) \\ z_2(k+1) = z_2(k) + T_{\mathrm{s}} \cdot \beta_2(U_{\mathrm{o}}(k) - z_1(k)) \end{cases} \quad (7)$$

where $z_1(k+1)$ and $z_2(k+1)$ are the observed output voltage and disturbance for $t=k+1$, respectively, $T_s=1/f_s$ is the control period, which is the same as the switching period in this article.

C. Online Coefficients Identification

In real applications, the characteristics of converters may vary due to factors, such as different working conditions, parameter change, or unconsidered disturbance [18]. Hence, developing an online updating data-driven model with identification techniques is of great significance, and this can be achieved through an effective coefficient identification method called FFRLS. In this design, the ESO illustrated in Part B generates the one-step ahead output voltage prediction value $z_1(k+1)$, which cannot be directly sampled at time $t=k$. Furthermore, $z_1(k+1)$ contributes to the calculation of the tracking error $\varepsilon(k+1)$ at $t=k$. This value, along with the regressor vector, is then used for coefficient identification, with the parameter vector updated online during each sampling period. This approach enhances the robustness and time delay compensation capabilities of the proposed controller.

First, the predicted voltage tracking error at $t=k+1$ is defined as (8), which also serves as the process output

$$\varepsilon(k+1)=z_1(k+1)-U_o^*(k+1) \tag{8}$$

where $\varepsilon(k+1)$ denotes the predicted output error with ESO. Here, the voltage reference at time $t=k+1$ can be approximated by $U_o^*(k)$ if the control period is small.

Furthermore, the aforementioned ARMA model is used for approximating the output error of system at time $t=k+1$, which can be written in the compact form as (9) (take $p=5$, $q=2$)

$$\hat{\varepsilon}(k+1)=X^T(k)\hat{\varphi}(k) \tag{9}$$

where the regressor vector at $t=k$ is defined as follows:

$$X(k)=[\varepsilon(k),\ldots,\varepsilon(k-4),1,\bar{u}(k+1),\bar{u}(k)]^T.$$

The parameter vector is shown as follows:

$$\hat{\varphi}(k)=[\phi_1(k),\ldots,\phi_5(k),\theta_0(k),\theta_1(k),\theta_2(k)]^T$$

and $\hat{\varepsilon}(k+1)$ means the tracking error approximated by the ARMA model.

It is obvious that the regressor vector $X(k)$ contains all the known data. Hence, the FFRLS algorithm can be used to online identify the coefficients in the data-driven model with the following recursive equation set:

$$\begin{cases}\hat{\varphi}(k+1)=\hat{\varphi}(k)+K(k+1)\left(\varepsilon(k+1)-X^T(k)\hat{\varphi}(k)\right)\\ K(k+1)=P(k)X(k)/(\lambda+X^T(k)P(k)X(k))\\ P(k+1)=(I-K(k+1)X^T(k))P(k)/\lambda\end{cases} \tag{10}$$

where λ is a tunable forgetting factor from (0,1). Note that, this factor should be chosen considering the comprise between the estimation performance and robustness [20].

The updated estimation results $\hat{\varphi}(k+1)$ above are then used for the control signal generation, which will be illustrated in detail in the next section.

D. Control Signal Generation

Assuming that the control period is sufficiently small and the DAB model varies relatively slowly, the coefficient vector acquired in $t=k$ can be regarded as unchanged in the adjacent control periods. Therefore, $\hat{\varphi}(k+1)$ from (10) can be used for one-step ahead tracking error prediction as follows:

$$\hat{\varepsilon}(k+2)=U_o(k+2)-U_o^*(k+2)\approx\hat{X}^T(k+1)\hat{\varphi}(k+1). \tag{11}$$

The predicted state vector $\hat{X}(k+1)$ is written as follows:

$$\hat{X}(k+1)=[\hat{\varepsilon}(k+1),\varepsilon(k),\ldots,\varepsilon(k-3)\ 1,\bar{u}(k+2),\bar{u}(k+1)]^T \tag{12}$$

where $\bar{u}(k+2)=u(k+1)$ denotes the control signal calculated in the kth control period.

The purpose of the predictive control is to manipulate the system output to track the reference in one step without any steady-state error. Hence, the cost function can be designed as follows:

$$J=(U_o(k+2)-U_o^*(k+2))^2=\hat{\varepsilon}(k+2)^2 \tag{13}$$

where $U_o^*(k+2)=U_o^*(k)$ can be assumed.

The control signal of the proposed MFPC method can be acquired by setting the partial derivative of the cost function (13) to be zero. Consequently, it can be expressed as follows:

$$\bar{u}(k+2)=-[\hat{\varepsilon}(k+1),\varepsilon(k),\varepsilon(k-1),\varepsilon(k-2)\ \varepsilon(k-3),1,0,\bar{u}(k+1)]\hat{\varphi}(k+1)/\theta_1(k+1). \tag{14}$$

Before implementing $\bar{u}(k+2)$ to the modulator, a low-pass filter (LPF) should be adopted to ensure a smooth performance and the filtered control signal $\bar{u}_{\text{filt}}(k+2)$ is given as follows:

$$\bar{u}_{\text{filt}}(k+2)=k_{\text{LPF}}\cdot\bar{u}(k+2)+(1-k_{\text{LPF}})\cdot\bar{u}(k+1) \tag{15}$$

where k_{LPF} is the filter coefficient to be tuned.

Ultimately, Fig. 4 summarizes and illustrates the aforementioned MFPC method.

IV. MFPC-APA Algorithm Implemented in DCTs

According to the analysis in Section III, this section introduces the implementation of the proposed method in DCTs, considering the characteristics and challenges of DCTs.

A. Adaptive Balance Controller for Input Voltage

For such ISOP-type DCTs, the accurate power sharing is essential for stable operations, which requires the relevant balance controller. It has been verified that the input voltage control is a sufficient condition rather than the output current control for the balance controller of ISOP-type DCTs [6]. To introduce the design of the proposed balance controller, the mechanism of voltage balance failure is discussed first.

The simplified equivalent schematic diagram of DCT is shown in Fig. 5(a) when the DCT is in the stable operation, which is also the equivalent operation point A in Fig. 5(b). Assuming that the total input voltage $\sum_{i=1}^{N}U_{\text{in}i}$ and the input current I_{in}

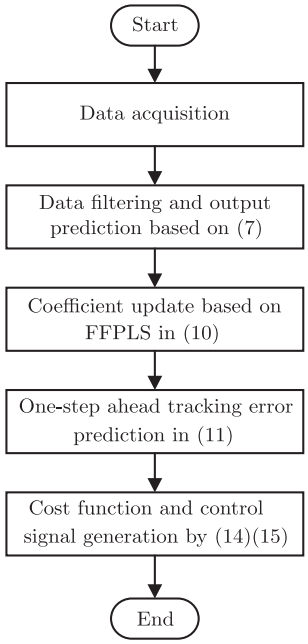

Fig. 4. Flowchart of the proposed MFPC method.

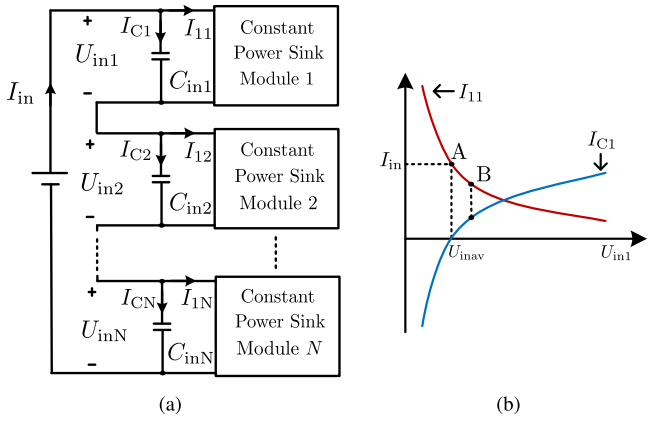

Fig. 5. Diagram for the mechanism of voltage balance failure. (a) Simplified equivalent schematic diagram of DCT. (b) Current of the input side of module 1.

are constant, and the initial voltage of submodules is balanced ($U_{\text{in}i} = U_{\text{inav}} = \frac{\sum_{i=1}^{N} U_{\text{in}i}}{N}$). When the input voltages of submodules are perturbed, e.g., U_{in1} is increase, U_{in2} is decrease, and others keep constant, I_{C1} will increase and I_{C2} will decrease. For module 1, this leads to that I_{11} decreases and the equivalent point moves from A to B. At point B, I_{11} is smaller than the input current I_{in}, causing that I_{C1} keeps rise and C_{in1} is still charged. The system will away from the initial point A and this process will continue until the system loses balance. Hence, a positive feedback loop is formed in the input voltage, making it impossible to resume to the balance point.

Therefore, to address this issue, an adjusting term based on the sigmoid function is proposed to create a nonlinear negative feedback. This adaptive term adjusts the output current (by control signal) of a certain submodule according to its input

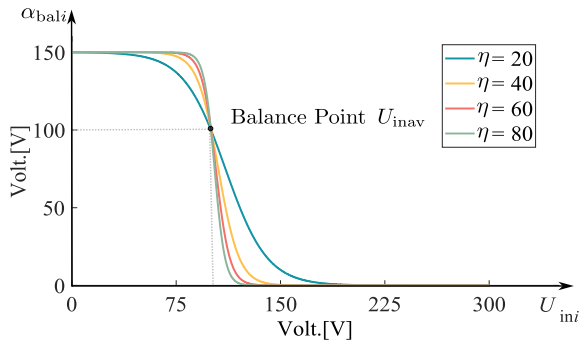

Fig. 6. Diagram of adjusting term.

voltage, thereby achieving the average power allocation and balancing the input voltage across all submodules. This adaptive controller enables less computational burden and higher robustness compared with the full MPC methods.

The balance controller can be implemented as follows:

$$\bar{u}_{\text{bal}i}(k+2) = \bar{u}_{\text{filt}}(k+2)\frac{U_{\text{in}i}(k)}{\alpha_{\text{bal}i}(k)} \tag{16}$$

where the $\bar{u}_{\text{bal}i}$ is the final control signal for modulation of the ith submodule, and the fraction term is the relevant adjusting term. For this adjusting term, $\alpha_{\text{bal}i}$ can be written as follows:

$$\alpha_{\text{bal}i}(k) = \frac{\sum_{i=1}^{N} U_{\text{in}i}(k)}{N-1}\left(\frac{-1}{1+e^{-\eta\left(\frac{U_{\text{in}i}(k)-\gamma_0(k)}{\sum_{i=1}^{N} U_{\text{in}i}(k)}\right)}}+1\right) \tag{17}$$

where η is the slope of the adjusting term and γ_0 is the mid-point of the sigmoid function and it can be derived as follows:

$$\gamma_0(k) = \left(\frac{\ln(N-1)}{-\eta} - \frac{1}{N}\right)\left(-\sum_{i=1}^{N} U_{\text{in}i}(k)\right). \tag{18}$$

To further introduce the adjusting term, Fig. 6 shows the diagram of $\alpha_{\text{bal}i}$ with various slope η, where $N = 3$ and $U_{\text{inav}} = 100$ V to meet the experimental condition. As it can be seen, when the input voltage of the ith submodule $U_{\text{in}i}$ is higher than the average input voltage U_{inav} ($U_{\text{in}i} > U_{\text{inav}}$), the adjusting term $\alpha_{\text{bal}i}$ moves down from 100 V. Similarly, when the input voltage of the ith submodule $U_{\text{in}i}$ is lower than the average input voltage U_{inav} ($U_{\text{in}i} < U_{\text{inav}}$), the adjusting term $\alpha_{\text{bal}i}$ moves up from 100 V. As shown in (16), this adjusts the gain of the system to $\bar{u}_{\text{filt}}(k+2)$. Taking submodule 1 as an example, in the case of $U_{\text{in1}} > U_{\text{inav}}$, $\alpha_{\text{bal1}} < 100$ V, and the gain $\frac{U_{\text{in1}}}{\alpha_{\text{bal1}}} > 1$, so that the control input $\bar{u}_{\text{bal1}}$ increases. Accordingly, I_{11} will increase. So far, it results in negative feedback. When the input current I_{in} is constant, I_{C1} will decrease, the system can move back to the equivalent operation point A.

B. Overall Implementation of Control Algorithms

Fig. 7 shows the block diagram of the proposed MFPC-APA scheme in the entire DCT system. The scheme mainly consists

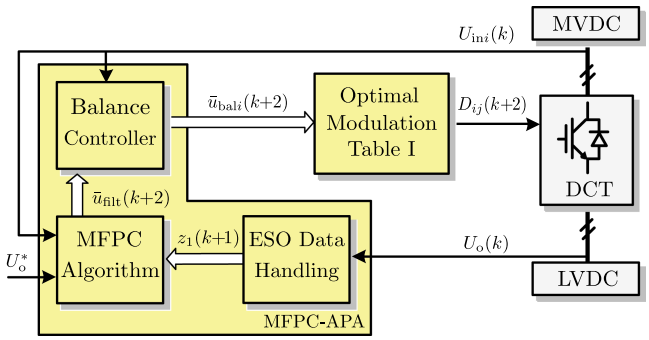

Fig. 7. Block diagram of the proposed MFPC-APA method.

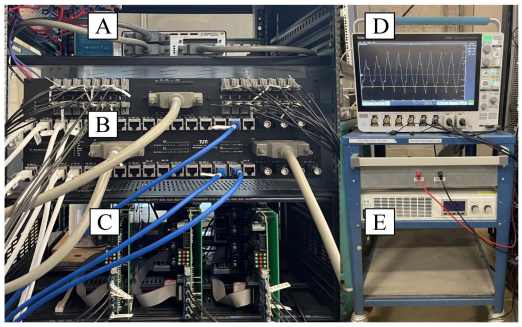

Fig. 8. DCT prototype for test. (a) PLECS real-time control system. (b) Signal interface. (c) DCT with three DABs. (d) Oscilloscope. (e) Power supply.

of two parts, i.e., the MFPC-APA algorithm and the optimal modulation. The former one further comprises the MFPC algorithm, ESO, and adaptive balance controllers. The filtered control signal $\bar{u}_{\mathrm{filt}}$ can be calculated as shown in Fig. 4. Then, the adaptive balance controllers [see (16)–(18)] adjust it according to the real-time input voltage of each submodule, achieving average power allocation and accurate input voltage balancing. Ultimately, the revised output signals $\bar{u}_{\mathrm{bal}i}(k+2)$ will be sent to the optimal modulation (see Table I). In the second part, based on the current range, the relevant optimal shift angles $D_{ij}(k+2), (i \in [1,2,\ldots,N]), (j \in [1,2,3])$ will be calculated and sent to the gate drivers system.

V. Experiments Results

A DCT prototype with three modules is built to verify the proposed method. Fig. 8 shows the prototype and the parameters are listed in Table II.

The performance of the proposed MFPC-APA method is experimentally compared with the PI-based method [16] and the conventional MPC method [10] in various cases including load step, reference step, accurate parameters cases, and inaccurate parameters cases.

Figs. 9–11 show the experimental results of three methods when the load steps. For the PI-based method, the parameters are tuned to be an optimized pair for no parameter mismatch case. The pretuned PI gains are multiplied by a parameter mismatch-related percentage to simulate the case when the pretuned controller encounters parameter change during operation.

TABLE II
Specifications and Parameters of Prototype

Parameter	Value
Input voltage	$U_{\mathrm{in}} = 300$ V
Output voltage	$U_{\mathrm{o}} = 80$ V
Number of modules	$N = 3$
Leakage inductor 1	$L_{\mathrm{k1}} = 106.71\ \mu$H
Leakage inductor 2	$L_{\mathrm{k2}} = 107.28\ \mu$H
Leakage inductor 3	$L_{\mathrm{k3}} = 108.44\ \mu$H
Ratio of transformers	$n_1 = n_2 = n_3 = 1$
Input capacitors	$C_{\mathrm{in1}} = C_{\mathrm{in2}} = C_{\mathrm{in3}} = 1\ m$F
Output capacitors	$C_{\mathrm{o1}} = C_{\mathrm{o2}} = C_{\mathrm{o3}} = 300\ \mu$F
Switching frequency	$f_{\mathrm{s}} = 10$ kHz

TABLE III
Steady-State Error of the Conventional MPC Method With $L'_{\mathrm{k1}} = 0.2L_{\mathrm{k1}}, L'_{\mathrm{k2}} = 0.5L_{\mathrm{k2}}$, and $L'_{\mathrm{k3}} = 0.8L_{\mathrm{k3}}$

	$U_{\mathrm{o}}^* = 80$ V (Light load)	$U_{\mathrm{o}}^* = 80$ V (Heavy load)	$U_{\mathrm{o}}^* = 60$ V
$U_{\mathrm{inav}} - U_{\mathrm{in1}}$	−6.01 V	−5.60 V	−6.08 V
$U_{\mathrm{inav}} - U_{\mathrm{in2}}$	−1.62 V	−2.03 V	−1.33 V
$U_{\mathrm{inav}} - U_{\mathrm{in3}}$	7.63 V	7.63 V	7.41 V
$U^* - U_{\mathrm{o}}$	1.70 V	3.34 V	1.41 V

Fig. 9 shows the results without any parameter mismatch. The output voltage U_{o} is controlled to a constant value U_{o}^*. The step of connected load results in that the required power is changed. Therefore, the output voltage U_{o} is forced to drop due to the instantaneous power gap. As can be seen, compared with the PI-based method (20.5 ms), the predictive control-based methods hold the faster recovery time, which is 4.4 and 4.1 ms for the conventional MPC method and the proposed MFPC-APA method. In all three methods, there is no obvious steady-state error in the controlled U_{o}. The input voltages of three submodules are balanced to their average voltage U_{inav} ($\frac{\sum_{i=1}^{N} U_{\mathrm{in}i}}{N} = \frac{300\,\mathrm{V}}{3} = 100\,\mathrm{V}$).

When it comes to parameter mismatches case, the same experimental conditions with setting leakage inductors mismatches ($L'_{\mathrm{k1}} = 0.2L_{\mathrm{k1}}, L'_{\mathrm{k2}} = 0.5L_{\mathrm{k2}}$, and $L'_{\mathrm{k3}} = 0.8L_{\mathrm{k3}}$) are shown in Fig. 10. The PI-based method holds the longest recovery time (20.7 ms), and the proposed MFPC-APA method presents the shortest recovery time (4.2 ms) without any static error in both input side and output side. The conventional MPC method shows the medium time (5.3 ms). However, its control performance suffers unacceptable deterioration. The error of output voltage $\Delta U_{\mathrm{o}} = U^* - U_{\mathrm{o}}$ is from 1.70 to 3.34 V. The transient response becomes slower compared with the no parameter error case. Also, the power of each module cannot be accurately allocated due to the inductors mismatches, which results in unbalanced input voltage. The relevant results in this case are summarized in Tables III and VI, where the light load represents $I_{\mathrm{o}} = 3.1$ A and the heavy load represents $I_{\mathrm{o}} = 7.8$ A. With the proposed MFPC-APA method, the steady-state error can be completely eliminated while similar dynamic performance remains.

Fig. 11 shows the case, where the leakage inductors are set as $L'_{\mathrm{k1}} = 1.7L_{\mathrm{k1}}, L'_{\mathrm{k2}} = 1.3L_{\mathrm{k2}}$, and $L'_{\mathrm{k3}} = 1.0L_{\mathrm{k3}}$. The PI-based method holds the longest recovery time (20.8 ms), and the proposed MFPC-APA method exhibits the shortest recovery

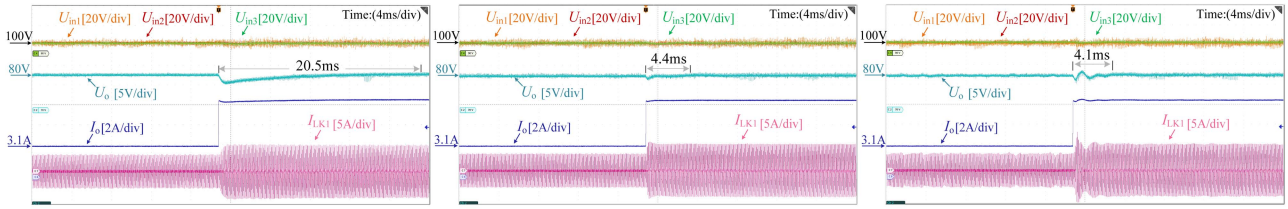

(a) (b) (c)

Fig. 9. Experimental waveform of load step without parameter mismatches. (a) PI method. (b) Conventional MPC method. (c) Proposed MFPC-APA method.

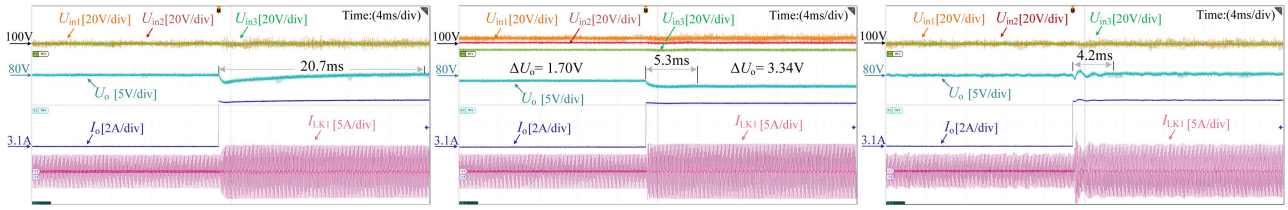

(a) (b) (c)

Fig. 10. Experimental waveform of load step with parameter mismatches ($L'_{\mathrm{k1}} = 0.2L_{\mathrm{k1}}$, $L'_{\mathrm{k2}} = 0.5L_{\mathrm{k2}}$, and $L'_{\mathrm{k3}} = 0.8L_{\mathrm{k3}}$). (a) PI method. (b) Conventional MPC method. (c) Proposed MFPC-APA method.

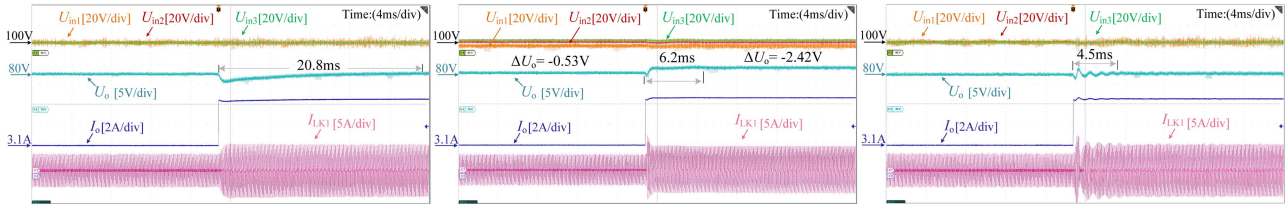

(a) (b) (c)

Fig. 11. Experimental waveform of load step with parameter mismatches ($L'_{\mathrm{k1}} = 1.7L_{\mathrm{k1}}$, $L'_{\mathrm{k2}} = 1.3L_{\mathrm{k2}}$, and $L'_{\mathrm{k3}} = 1.0L_{\mathrm{k3}}$). (a) PI method. (b) Conventional MPC method. (c) Proposed MFPC-APA method.

TABLE IV
STEADY-STATE ERROR OF THE CONVENTIONAL MPC METHOD WITH $L'_{\mathrm{k1}} = 1.7L_{\mathrm{k1}}$, $L'_{\mathrm{k2}} = 1.3L_{\mathrm{k2}}$, AND $L'_{\mathrm{k3}} = 1.0L_{\mathrm{k3}}$

	$U_{\mathrm{o}}^* = 80$ V (Light load)	$U_{\mathrm{o}}^* = 80$ V (Heavy load)	$U_{\mathrm{o}}^* = 60$ V
$U_{\mathrm{inav}} - U_{\mathrm{in1}}$	3.73 V	4.28 V	3.82 V
$U_{\mathrm{inav}} - U_{\mathrm{in2}}$	−1.18 V	−0.37 V	−1.18 V
$U_{\mathrm{inav}} - U_{\mathrm{in3}}$	−2.55 V	−1.95 V	−2.56 V
$U^* - U_{\mathrm{o}}$	−0.53 V	−2.42 V	−0.26 V

TABLE V
TRANSIENT RESPONSE TIME OF U_{o} OF THREE METHODS WITHOUT MISMATCHES

	Load step	Reference step
PI method	20.5 ms	37.4 ms
Conventional MPC method	4.4 ms	11.4 ms
MFPC-APA method	4.1 ms	12.9 ms

TABLE VI
TRANSIENT RESPONSE TIME OF U_{o} OF THREE METHODS WITH $L'_{\mathrm{k1}} = 0.2L_{\mathrm{k1}}$, $L'_{\mathrm{k2}} = 0.5L_{\mathrm{k2}}$, AND $L'_{\mathrm{k3}} = 0.8L_{\mathrm{k3}}$

	Load step	Reference step
PI method	20.7 ms	37.6 ms
Conventional MPC method	5.3 ms	13.8 ms
MFPC-APA method	4.2 ms	12.9 ms

TABLE VII
TRANSIENT RESPONSE TIME OF U_{o} OF THREE METHODS WITH $L'_{\mathrm{k1}} = 1.7L_{\mathrm{k1}}$, $L'_{\mathrm{k2}} = 1.3L_{\mathrm{k2}}$, AND $L'_{\mathrm{k3}} = 1.0L_{\mathrm{k3}}$

	Load step	Reference step
PI method	20.8 ms	37.9 ms
Conventional MPC method	6.2 ms	15.2 ms
MFPC-APA method	4.5 ms	13.4 ms

time (4.5 ms) without any static error in both input side and output side. The results of the conventional MPC method reveal the similar characters to the former case, including the impeded recovery time (6.2 ms), the errors of output voltage (ΔU_{o} is from -0.53 to -2.42 V) and input voltage. The relevant results are summarized in Tables IV and VII.

Next, the experimental results of reference steps are shown in Figs. 12–14. Such steps require promptly and accurately controlling the changed power in an instant.

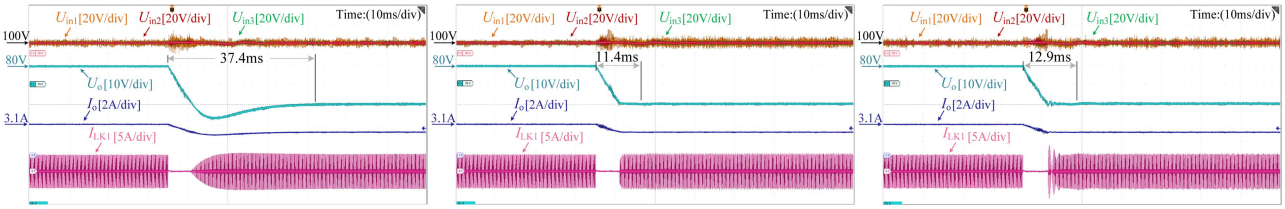

Fig. 12. Experimental waveform of reference step without parameter mismatches. (a) PI method. (b) Conventional MPC method. (c) Proposed MFPC-APA method.

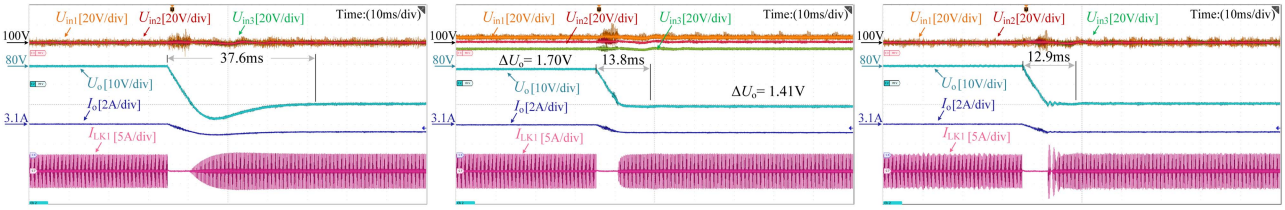

Fig. 13. Experimental waveform of reference step with parameter mismatches ($L'_{k1} = 0.2L_{k1}, L'_{k2} = 0.5L_{k2}$, and $L'_{k3} = 0.8L_{k3}$). (a) PI method. (b) Conventional MPC method. (c) Proposed MFPC-APA method.

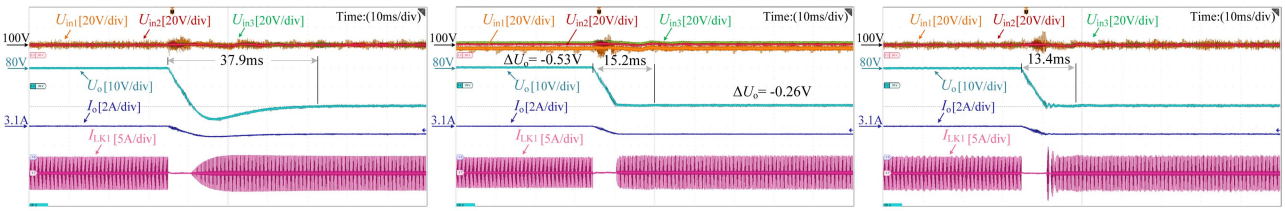

Fig. 14. Experimental waveform of reference step with parameter mismatches ($L'_{k1} = 1.7L_{k1}, L'_{k2} = 1.3L_{k2}$, and $L'_{k3} = 1.0L_{k3}$). (a) PI method. (b) Conventional MPC method. (c) Proposed MFPC-APA method.

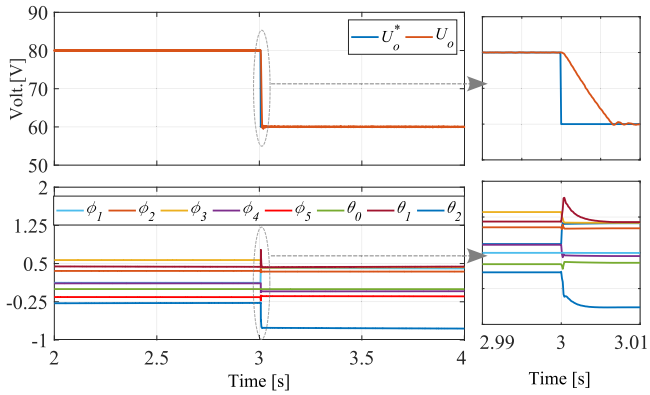

Fig. 15. Experimental measurement of estimated parameter vector under reference step case.

Fig. 12 shows the results without any parameter mismatch. As can be seen, the PI-based method still spends the longest time (37.4 ms) to track the new reference and it leads to a high overshoot (7.41 V). The predictive control-based methods spend much shorter time without overshoot (11.4 ms for the conventional MPC method and 12.9 ms for the proposed MFPC-APA method). Meanwhile, no obvious static error can be found in all three methods.

In Fig. 13, where the $L'_{k1} = 0.2L_{k1}, L'_{k2} = 0.5L_{k2}$, and $L'_{k3} = 0.8L_{k3}$, the conventional MPC method presents steady-state errors in output voltage U_o (ΔU_o is from 1.41 to 1.70 V) and input voltage. Its transient performance (13.8 ms) is prolonged

due to the large parameter mismatches. For the proposed MFPC-APA method, the fastest tracking time (12.9 ms) is achieved and no steady-state error can be found.

Fig. 14, where the $L'_{k1} = 1.7L_{k1}$, $L'_{k2} = 1.3L_{k2}$, and $L'_{k3} = 1.0L_{k3}$, shows the similar results as those in Fig. 13.

Based on the comprehensive comparison results from Figs. 9–14, the performance of the three methods can be summarized from Tables III to VII, where Tables III and IV conclude the conventional MPC method's steady-state error while Tables V–VII compare the response time of transient for all the working conditions.

As it can be seen, the proposed method achieves accurate power allocation and voltage regulation for the input and output sides while keeping fast dynamic performance.

Besides, the experimental measurement of the estimated parameter vector in (9) under voltage reference step condition is visualized by Fig. 15. As can be seen, all the parameters can converge to a certain value in the steady state and the system remains stable after the reference sudden change, which proves the feasibility and robustness of the proposed method.

Lastly, as shown in Figs. 9–14, the steady-state power quality of the output voltage and current using the proposed method is nearly the same as that of the compared methods. However, the proposed method does not exhibit steady-state errors in the presence of parameter mismatches.

VI. Conclusion

In this article, we proposed an MFPC based on ARMA structure for ISOP-type DCTs consisting of DABs. Combined with the proposed adaptive balance controller, this method achieves accurate power/voltage allocation among all submodules while keeping fast dynamic performance. The ARMA structure is analyzed, followed with the detailed method to select the relevant orders of coefficients. Coordinating with the FFRLS scheme, the proposed MFPC-APA method completely gets rid of all the electrical parameters so that strong robustness can be guaranteed. In addition, an ESO is presented to clean the sampled data and reduce the data-driven model's order in the one-step delay compensation design. Then, the mechanism of voltage balance failure is discussed. Accordingly, the novel adaptive balance controller is introduced, which efficiently balances the input voltage with less computational burden compared with full MPC methods. The experimental results demonstrate that the proposed MFPC-APA method regulates the input and output sides with higher robustness and maintains fast dynamic response.

References

[1] R. Zhu, M. Liserre, M. Langwasser, and C. Kumar, "Operation and control of the smart transformer in meshed and hybrid grids: Choosing the appropriate smart transformer control and operation scheme," *IEEE Ind. Electron. Mag.*, vol. 15, no. 1, pp. 43–57, Mar. 2021.

[2] L. Zheng, R. P. Kandula, and D. Divan, "Current-source solid-state DC transformer integrating LVDC microgrid, energy storage, and renewable energy into MVDC grid," *IEEE Trans. Power Electron.*, vol. 37, no. 1, pp. 1044–1058, Jan. 2022.

[3] H. Weng, J. Li, K. Shi, M. Chen, P. T. Krein, and D. Xu, "A DC solid-state transformer with DC fault ride-through capability," *IEEE Trans. Emerg. Sel. Topics Power Electron.*, vol. 10, no. 4, pp. 3617–3630, Aug. 2022.

[4] Y. Zhuang et al., "A multiport DC solid-state transformer for MVDC integration interface of multiple distributed energy sources and DC loads in distribution network," *IEEE Trans. Power Electron.*, vol. 37, no. 2, pp. 2283–2296, Feb. 2022.

[5] M. Liserre, M. A. Perez, M. Langwasser, C. A. Rojas, and Z. Zhou, "Unlocking the hidden capacity of the electrical grid through smart transformer and smart transmission," *Proc. IEEE*, vol. 111, no. 4, pp. 421–437, Apr. 2023.

[6] W. Chen, X. Ruan, H. Yan, and K. T. Chi, "DC/DC conversion systems consisting of multiple converter modules: Stability, control, and experimental verifications," *IEEE Trans. Power Electron.*, vol. 24, no. 6, pp. 1463–1474, Jun. 2009.

[7] Z. Lu, G. Xu, M. Su, Y. Liao, Y. Liu, and Y. Sun, "Stability analysis and design of common phase shift control for input-series output-parallel dual active bridge with consideration of dead-time effect," *IEEE Trans. Emerg. Sel. Topics Power Electron.*, vol. 10, no. 6, pp. 7721–7732, Dec. 2022.

[8] H. Zhang et al., "Extended-state-observer based model predictive control of a hybrid modular DC transformer," *IEEE Trans. Ind. Electron.*, vol. 69, no. 2, pp. 1561–1572, Feb. 2022.

[9] T. Geyer, *Model Predictive Control of High Power Converters and Industrial Drives*. Hoboken, NJ, USA: Wiley, 2016.

[10] H. Zhang et al., "Model predictive control of input-series output-parallel dual active bridge converters based DC transformer," *IET Power Electron.*, vol. 13, no. 6, pp. 1144–1152, 2020.

[11] D. Kong, X. Gao, Z. Zhang, C. Liu, M. L. Heldwein, and R. Kennel, "Minimization of current stress for dual active bridge converters based on model predictive control with enhanced ZVS ability," *IEEE Trans. Ind. Electron.*, vol. 71, no. 8, pp. 8970–8980, Aug. 2024.

[12] D. Kong, Z. Zhang, C. Liu, W. Tian, X. Gao, and R. Kennel, "Modulated model predictive control of power electronics transformer based on isolated modular multilevel converter," in *2021 IEEE Int. Conf. Predictive Control Elect. Drives Power Electron.*. IEEE, 2021, pp. 831–835.

[13] L. Chen, S. Shao, Q. Xiao, L. Tarisciotti, P. W. Wheeler, and T. Dragičević, "Model predictive control for dual-active-bridge converters supplying pulsed power loads in naval DC micro-grids," *IEEE Trans. Power Electron.*, vol. 35, no. 2, pp. 1957–1966, Feb. 2020.

[14] Z. Guo, Y. Luo, and K. Sun, "Parameter identification of the series inductance in DAB converters," *IEEE Trans. Power Electron.*, vol. 36, no. 7, pp. 7395–7399, Jul. 2021.

[15] Y. Wang, Y. Guan, O. B. Fosso, M. Molinas, S.-Z. Chen, and Y. Zhang, "An input-voltage-sharing control strategy of input-series-output-parallel isolated bidirectional DC/DC converter for DC distribution network," *IEEE Trans. Power Electron.*, vol. 37, no. 2, pp. 1592–1604, Feb. 2022.

[16] S. Pugliese, G. Buticchi, R. A. Mastromauro, M. Andresen, M. Liserre, and S. Stasi, "Soft-start procedure for a three-stage smart transformer based on dual-active bridge and cascaded H-bridge converters," *IEEE Trans. Power Electron.*, vol. 35, no. 10, pp. 11039–11052, Oct. 2020.

[17] Y. Wu, M. H. Mahmud, Y. Zhao, and H. A. Mantooth, "Uncertainty and disturbance estimator-based robust tracking control for dual-active-bridge converters," *IEEE Trans. Transp. Electrific.*, vol. 6, no. 4, pp. 1791–1800, Dec. 2020.

[18] Y. Zhu et al., "Model predictive control with a novel parameter identification scheme for dual-active-bridge converters," *IEEE Trans. Emerg. Sel. Topics Power Electron.*, vol. 11, no. 5, pp. 4704–4713, Oct. 2023.

[19] Y. Wei, F. Wang, H. Young, D. Ke, and J. Rodríguez, "Autoregressive moving average model-free predictive current control for PMSM drives," *IEEE Trans. Emerg. Sel. Topics Power Electron.*, vol. 11, no. 4, pp. 3874–3884, Aug. 2023.

[20] F. Wang, Y. Wei, H. Young, D. Ke, D. Huang, and J. Rodríguez, "Continuous-control-set model-free predictive control using time-series subspace for PMSM drives," *IEEE Trans. Ind. Electron.*, vol. 71, no. 7, pp. 6656–6666, Jul. 2024.

[21] Y. Wei, H. Young, F. Wang, and J. Rodríguez, "Generalized data-driven model-free predictive control for electrical drive systems," *IEEE Trans. Ind. Electron.*, vol. 70, no. 8, pp. 7642–7652, Aug. 2023.

[22] Y. Zhang, J. Jin, and L. Huang, "Model-free predictive current control of PMSM drives based on extended state observer using ultralocal model," *IEEE Trans. Ind. Electron.*, vol. 68, no. 2, pp. 993–1003, Feb. 2021.

[23] P. G. Ipoum-Ngome, D. L. Mon-Nzongo, R. C. C. Flesch, J. Song-Manguelle, M. Wang, and T. Jin, "Model-free predictive current control for multilevel voltage source inverters," *IEEE Trans. Ind. Electron.*, vol. 68, no. 10, pp. 9984–9997, Oct. 2021.
[24] S. Saadatmand, P. Shamsi, and M. Ferdowsi, "Power and frequency regulation of synchronverters using a model free neural network-based predictive controller," *IEEE Trans. Ind. Electron.*, vol. 68, no. 5, pp. 3662–3671, May 2021.
[25] N. Hou and Y. W. Li, "Overview and comparison of modulation and control strategies for a nonresonant single-phase dual-active-bridge DC–DC converter," *IEEE Trans. Power Electron.*, vol. 35, no. 3, pp. 3148–3172, Mar. 2020.
[26] M. Capó-Lliteras, G. G. Oggier, E. Bullich-Massagué, D. Heredero-Peris, and D. Montesinos-Miracle, "Analytical and normalized equations to implement the optimized triple phase-shift modulation strategy for DAB converters," *IEEE J. Emerg. Sel. Topics Power Electron.*, vol. 11, no. 3, pp. 3535–3546, Jun. 2023.
[27] G. E. Box, G. M. Jenkins, G. C. Reinsel, and G. M. Ljung, *Time Series Analysis: Forecasting and Control*. Hoboken, NJ, USA: Wiley, 2015.
[28] P. D. Lellis, F. L. Iudice, and N. Pasquino, "Time-series-based model and validation for prediction of exposure to wideband radio frequency electromagnetic radiation," *IEEE Trans. Instrum. Meas.*, vol. 69, no. 6, pp. 3198–3205, Jun. 2020.

Dehao Kong (Graduate Student Member, IEEE) received the B.S. and M.S. degrees in electrical engineering from Northeast Electric Power University, Jilin, China, in 2017 and 2020, respectively. He is currently working toward the Ph.D. degree in electrical engineering with the Chair of High-Power Converter Systems and the Chair of Electrical Drive Systems and Power Electronics, Technical University of Munich, Munich, Germany.

His research interests include dc/dc converters, solid-state transformers, and advanced control methods for power electronics.

Shaobin Li was born in Liaoning Province, China, in 1997. He received the B.S degree in electrical engineering in 2019 from the Harbin Institute of Technology, Harbin, China, where he is currently working toward the Ph.D degree in electrical engineering with the School of Electrical Engineering and Automation.

His current research focuses on permanent magnet motor drives and control.

Chuang Liu (Member, IEEE) received the Ph.D. degree in electrical engineering from the Harbin Institute of Technology, Harbin, China, in 2013.

From 2010 to 2012, he was with the Future Energy Electronics Center, Virginia Polytechnic Institute and State University, Blacksburg, USA, as a Visiting Ph.D. Student. In 2013, he became an Associate Professor with the School of Electrical Engineering, Northeast Electric Power University, Jilin, China, where he has been a Full Professor since 2016. His research interests include power-electronics-based transformers for future hybrid power grids and power-electronics-based power system stability analysis and control.

Zhenbin Zhang (Senior Member, IEEE) received the Ph.D. degree in electrical and energy engineering from the Technical University of Munich, Munich, Germany, in 2016.

He was a Postdoctoral Researcher of Electrical and Energy Engineering with the Technical University of Munich. Since 2017, he has been a Full Professor with Shandong University, Jinan, China, where he is currently the Director of both the Laboratory of More Power Electronics Energy Systems and the Institute of Sustainable Energy and Smart Grids. His research interests include power electronics and electrical drives, sustainable energy systems, and micro-grids.

Dr. Zhang was the recipient of the VDE Award 2017 in Suedbayern, Germany. He is an Associate Editor for IEEE TRANSACTIONS ON POWER ELECTRONICS. He is an IET Fellow Member and IET Chartered Engineer.

Yuanxiang Sun (Graduate Student Member, IEEE) received the B.S. degree in electrical engineering from the China University of Mining and Technology, Xuzhou, China, in 2019, and the M.S. degree in electrical engineering from Shandong University, Jinan, China, in 2022. He is currently working toward the Ph.D. degree in electrical engineering with the Chair of High-Power Converter Systems, Technical University of Munich, Munich, Germany.

His research interests include advanced control of grid-connected converters and grid integration of offshore wind power.

Ralph Kennel (Life Senior Member, IEEE) received the diploma and Dr. Ing. (Ph.D.) degrees in electrical engineering from the University of Kaiserslautern, Kaiserslautern, Germany, in 1979 and 1984, respectively.

From 1983 to 1999, he worked with Robert BOSCH GmbH, Gerlingen, Germany, and was responsible for the development of servo drives. From 1999 to 2008, he was a Professor of Electrical Machines and Drives with Wuppertal University, Wuppertal, Germany. Since 2008, he has been the Head of the Chair of Electrical Drive Systems and Power Electronics with the Technical University of Munich, Munich, Germany. His research interests include renewable energy, sensorless control of ac drives, predictive control of power electronics, and hardware-in-the-loop systems.

Dr. Kennel was the recipient of the EPE Outstanding Achievement Award. He is a Fellow of IET and a Chartered Engineer in the U.K. Within IEEE he was Treasurer of the Germany Section as well as ECCE Global Partnership Chair of the Power Electronics Society.

Marcelo Lobo Heldwein (Senior Member, IEEE) received the B.S. and M.S. degrees in electrical engineering from the Federal University of Santa Catarina (UFSC), Florianópolis, Brazil, in 1997 and 1999, respectively, and the Ph.D. degree in electrical engineering from the Swiss Federal Institute of Technology (ETH Zürich), Zurich, Switzerland, in 2007.

He is currently the Head of the Chair of High-Power Converter Systems, Technical University of Munich, Munich, Germany. From 1999 to 2003, he was with industry, including R&D activities with the Power Electronics Institute, Florianópolis, Brazil, and Emerson Network Power, in Brazil and Sweden. From 2007 to 2009, he was a Postdoctoral Fellow with ETH Zürich and UFSC. From 2010 to 2022, he was a Professor with the Department of Electronics and Electrical Engineering, UFSC. His research interests include power electronics, advanced power distribution technologies, and electromagnetic compatibility.

Dr. Heldwein is a Member of the Brazilian Power Electronic Society and a Member of the Advisory Board of PCIM Europe.